

# Dielectric elastomer energy harvesting: maximal converted energy, viscoelastic dissipation and a wave power generator

Xiongfei Lv<sup>1</sup>, Liwu Liu<sup>1</sup>, Yanju Liu<sup>1</sup> and Jinsong Leng<sup>2</sup>

<sup>1</sup>Department of Astronautic Science and Mechanics, Harbin Institute of Technology (HIT), PO Box 301, No. 92 West Dazhi Street, Harbin 150001, People's Republic of China

<sup>2</sup>Centre for Composite Materials and Structures, Science Park of Harbin Institute of Technology (HIT), PO Box 3011, No. 2 Yikuang Street, Harbin 150080, People's Republic of China

E-mail: [yj\\_liu@hit.edu.cn](mailto:yj_liu@hit.edu.cn) and [lengjs@hit.edu.cn](mailto:lengjs@hit.edu.cn)

Received 21 April 2015, revised 22 August 2015

Accepted for publication 7 September 2015

Published DD MM 2015



CrossMark

## Abstract

Dielectric elastomer (DE) is a smart soft material. It is able to produce large deformation under mechanical force and electric field, so that it can achieve mutual conversion between mechanical energy and electrical energy. Based on this property, dielectric elastomer can be used in energy harvesting field. In this paper, firstly, we analyzed the constitutive relation under different hyperelastic models (Gent and neo-Hookean model) based on both theoretical and experimental study. Secondly, we depicted the allowable areas in force-displacement and voltage-charge plane according to different failure modes, and then calculated the maximal energy density in one energy harvesting period. Thirdly, we studied the viscoelastic energy dissipation which can lose the input mechanical energy in the energy harvesting process. Finally, we designed and fabricated a wave power generator, and tested its performance. This paper is of deep significance to the future applications of DE generators.

Keywords: dielectric elastomer, dissipation, generator, converted energy

SQ1 (Some figures may appear in colour only in the online journal)

## 1. Introduction

Energy, one of the most important driving forces for the development of the world, has always played an important role in the history of human civilization. However, with the rapid development of the world, energy shortage and environmental pollution have become major problems that threaten human society. How to solve these problems? Looking for renewable and clean energy has become the major objective of scientific researchers. So far, the use of solar energy, wind energy, water energy, etc, has become the strategic frontier to which the scientific researchers are devoted. The defects of hard materials and inspiration from bionics have promoted the rapid development of smart soft materials. Dielectric elastomer (DE) is one of them. It belongs to a kind of electro-active polymers (EAPs) [1–3]. It possesses advantages such as good biological compatibility, high elastic energy density, fast

response, light weight, low price, easy processing and manufacturing, etc [4, 5].

In energy harvesting, the essence of DE is a variable capacitor; here we consider a DE film with compliant electrodes (such as carbon, graphite, etc) evenly coated on its two opposite surfaces. As shown in figure 1: first, we charge and stretch the film, the initial mechanical and electrical energy are inputted into the system; second, we turn off the power to maintain the charge on the film constant, and third, we relax the film to its original shape. During the shape recover process, the capacitance of DE film will decrease. As a result, the voltage across the DE film will increase. With the same charge and higher voltage, the initial input electrical energy will increase. In summary, the energy harvesting principle utilizes mechanical energy to raise electrical energy from a lower level to a higher level [6, 7].

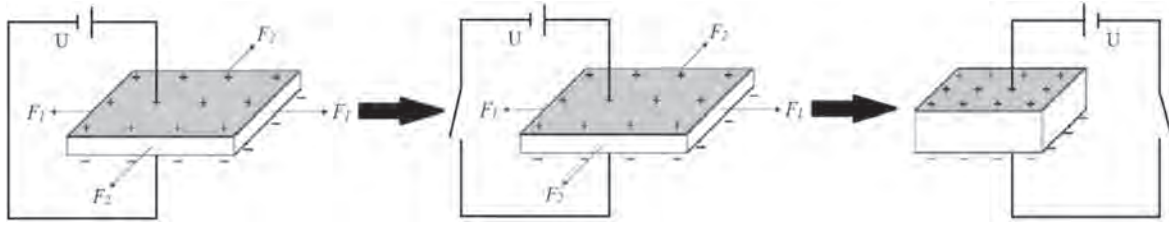


Figure 1. Operating Principle of Energy Harvesting.

Based on thermodynamics and continuum mechanics, Suo has established the theory of dielectric elastomer [8]. Following his work, coexistent states, instability, large deformation, optimization design, dynamics, finite element method and nonequilibrium have been widely studied [9–20]. In this paper, we studied the converted energy and energy dissipation, then designed a generator.

As the core component of energy harvesting, the property of DE material determines the ability to convert energy. DE is a hyperelastic material whose mechanical properties are sensitive to time, environmental conditions, strain history, loading rate and strain rate. And hardening or softening phenomenon also appears. Therefore, the material nonlinearity and the geometrical nonlinearity must be taken into account when one tries to establish the constitutive relation of DE materials. Since the 19th century, researchers have set up numerous constitutive models based on different theories. Gent model and neo-Hookean model are two commonly used hyperelastic energy models. Through comparison of the two models, we first investigated the mechanical property of DE material.

Maximal converted energy reflects the performance of a DE generator. Allowable area is a graphical method to calculate the value. Using neo-Hookean model, Koh *et al* obtained an ideal maximal energy density of  $6.3 \text{ J g}^{-1}$ . In addition, they also proposed a rectangular energy harvesting cycle [21]. It can transfer electrical energy from a low-voltage power supply to a high-voltage power supply through mechanical work and has been already realized in laboratory [21, 22]. Liu *et al* analyzed the problem using the Mooney-Rivlin model, they also considered unequal-biaxial stretch [23]. But the hyperelastic energy model they chose cannot describe the strain hardening phenomenon that often appears in DE materials, and they also did not calculate the maximal converted energy of the rectangular cycle they proposed. Therefore, following their work, the ideal and rectangular maximal converted energy were analyzed by Gent model.

DE materials have typical viscoelastic effect. Due to the time-dependent forces applied in energy harvesting, the viscoelastic behavior affects the performance of a DE generator. Hong established a mechanical model of viscoelastic dielectrics, and analyzed the instability [24]. Foo *et al* established the dissipative DE model and analyzed the electromechanical behavior of dissipative DEs under different conditions [25], and further studied the energy dissipation of the rectangular cycle [26]. Li *et al* analyzed the energy dissipation behavior of an inflatable DE generator considering inhomogeneous

field [27]. Among these studies, the fundamental cycle (as explained in figure 1) was not involved. Therefore, this work was done in the paper.

Based on the working principle, DE is especially suitable for harvesting energy from human motion, ocean and river [28, 29]. DARPA developed a generator to harvest the energy generated by walking soldiers [29]. Chiba *et al* developed a proof-of-concept water mill that can harvest energy from simulated flowing river in laboratory [30], and they further developed a buoy generator to harvest energy from ocean waves. This buoy generator uses a proof-mass to provide mechanical force that stretches and contracts the DE material [30]. Maas and Graf developed a novel flow energy generator which consists of a DE tube with a closing mechanism on the outlet [31]. Inspired by Chiba's work, we designed a small wave power generator which utilizes hammers connected to the bottom to provide mechanical force. The aim of this work is to verify the energy harvesting principle and to achieve the conversion. It is significant for the further design of DE generator.

## 2. Dielectric elastomer

DE materials are thought to be incompressible. They are composed of mutual cross-linked polymer molecular chains which have finite length. When under no load, the polymer chains are curly, and there are a large number of possible configurations. When under loads, the polymer chains are stretched and gradually approach the limited configuration. When near the limiting stretch, the tensile modulus increases sharply, which is the strain hardening phenomenon. Gent model can describe this phenomenon [32].

$$W(\lambda_1, \lambda_2) = -\frac{\mu}{2} J_{\text{lim}} \ln \left( 1 - \frac{\lambda_1^2 + \lambda_2^2 + \lambda_1^{-2} \lambda_2^{-2} - 3}{J_{\text{lim}}} \right) \quad (1)$$

Where  $\mu$  is small deformation shear modulus,  $J_{\text{lim}} = \lambda_{1 \text{ lim}}^2 + \lambda_{2 \text{ lim}}^2 + \lambda_{1 \text{ lim}}^{-2} \lambda_{2 \text{ lim}}^{-2} - 3$  is a constant which is relative to limiting stretch.

When under small stretch, that is  $(\lambda_1^2 + \lambda_2^2 + \lambda_1^{-2} \lambda_2^{-2} - 3)/J_{\text{lim}} \rightarrow 0$ , the Taylor expansion of Gent model is

$$W(\lambda_1, \lambda_2) = \frac{\mu}{2} (\lambda_1^2 + \lambda_2^2 + \lambda_1^{-2} \lambda_2^{-2} - 3) \quad (2)$$

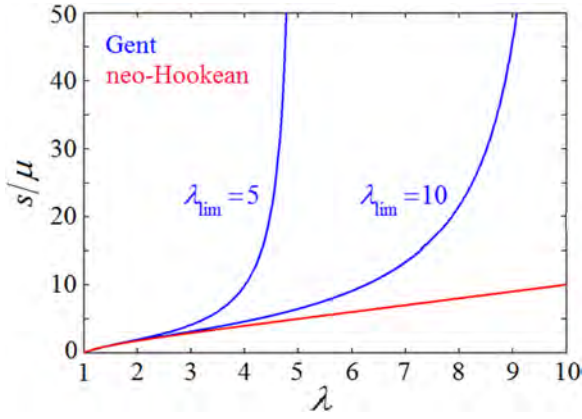


Figure 2. Nominal Stress-Stretch Curves.

This is neo-Hookean model which is the most commonly used molecular statistical constitutive model. Compared with Gent model, it has a much simpler form.

When under uniaxial stretch, the relations between nominal stress and stretch of the DE film by the two models are

$$\frac{s}{\mu} = \frac{J_{\text{lim}}(\lambda - \lambda^{-2})}{J_{\text{lim}} - \lambda^2 - 2/\lambda + 3} \quad (3)$$

$$\frac{s}{\mu} = \lambda - \lambda^{-2} \quad (4)$$

where

$$J_{\text{lim}} = \lambda_{\text{lim}}^2 + \frac{2}{\lambda_{\text{lim}}} - 3 \quad (5)$$

When under electric field, the DE deforms equal-biaxially, and the relations between nominal electric field and stretch by the two models are

$$\frac{\tilde{E}}{\sqrt{\mu/\varepsilon}} = \left[ \frac{J_{\text{lim}}(\lambda^{-2} - \lambda^{-8})}{J_{\text{lim}} - 2\lambda^2 - \lambda^{-4} + 3} \right]^{\frac{1}{2}} \quad (6)$$

$$\frac{\tilde{E}}{\sqrt{\mu/\varepsilon}} = (\lambda^{-2} - \lambda^{-8})^{\frac{1}{2}} \quad (7)$$

where

$$J_{\text{lim}} = 2\lambda_{\text{lim}}^2 + \lambda_{\text{lim}}^{-4} - 3 \quad (8)$$

Here we choose  $\lambda_{\text{lim}} = 5$  and  $\lambda_{\text{lim}} = 10$ . In figures 2 and 3, the blue curves represent Gent model, while the red curves represent neo-Hookean model.

From figure 2, different  $\lambda_{\text{lim}}$  in Gent model corresponds to a different curve, and each curve has a limit at  $\lambda_{\text{lim}}$ . The three curves are nearly identical under small stretch, and the overlapping scope increases as  $\lambda_{\text{lim}}$  increases. From figure 3, Gent model has two extreme points, but neo-Hookean model has only one. The maximal value which differs slightly represents the instability point. But Gent model stiffens at  $\lambda_{\text{lim}}$  after instability. The three curves are also nearly identical

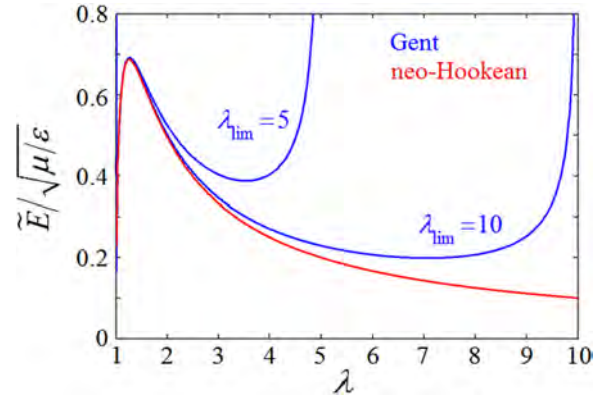


Figure 3. Voltage-Stretch Curves.

under small stretch, and the overlapping scope increases as  $\lambda_{\text{lim}}$  increases.

Next we conduct a uniaxial tensile test. The DE material is TC 5005 A/B-C produced by BJB Enterprises, Inc., USA. It is a room temperature curing polydimethyl siloxane with three components. Component A is silicone rubber base; component B is catalyst; and component C is silicone fluid. TC-5005 A/B is processed by adding curing agent B at a ratio of 10 parts by weight to 100 parts by weight of A. Component C can be added as much as 50% to the total weight of TC-5005 A/B. It affects the modulus of the silicon rubber. To reflect the difference, 20% and 40% are chosen.

The test specimen size is shown in figure 4(a). The test was done on Zwick Z010 with the loading rate  $200 \text{ mm min}^{-1}$ . We test five specimens for each material. To compare the theoretical and test curves, here we employ a simple method to fit the unknown parameter. The small deformation shear modulus is the same for a certain material in both models. We can use neo-Hookean model because of its simple form. From equation (4), by setting  $\lambda - \lambda^{-2}$  to be the x-coordinate and  $s$  to be the y-coordinate, the slope of the linear region can be approximately seen as the value of  $\mu$ . Table 1 is the data fitting result.

Eliminating error data, data fitting results and Mooney plot are shown in figures 4(b)–(e). The green curves represent Gent model, and the red curves represent neo-Hookean model, while the blue curves represent the test results. The test curves of 40% silicone rubber have a large deviation. It may be caused by our material preparation technique (mixing unevenly, placing inequality, etc). Both the two models cannot match well under large stretch. Therefore, if characterizing the material property under small stretch, the neo-Hookean model is better because of its simplicity. However, due to the fact that Gent model can describe the strain hardening phenomenon, its trend is in accordance with the five test curves, so the error is smaller. But it still has a certain gap.

### 3. Maximal converted energy

When characterizing the material property under large stretch, Gent model is more accurate. For a DE generator, a larger

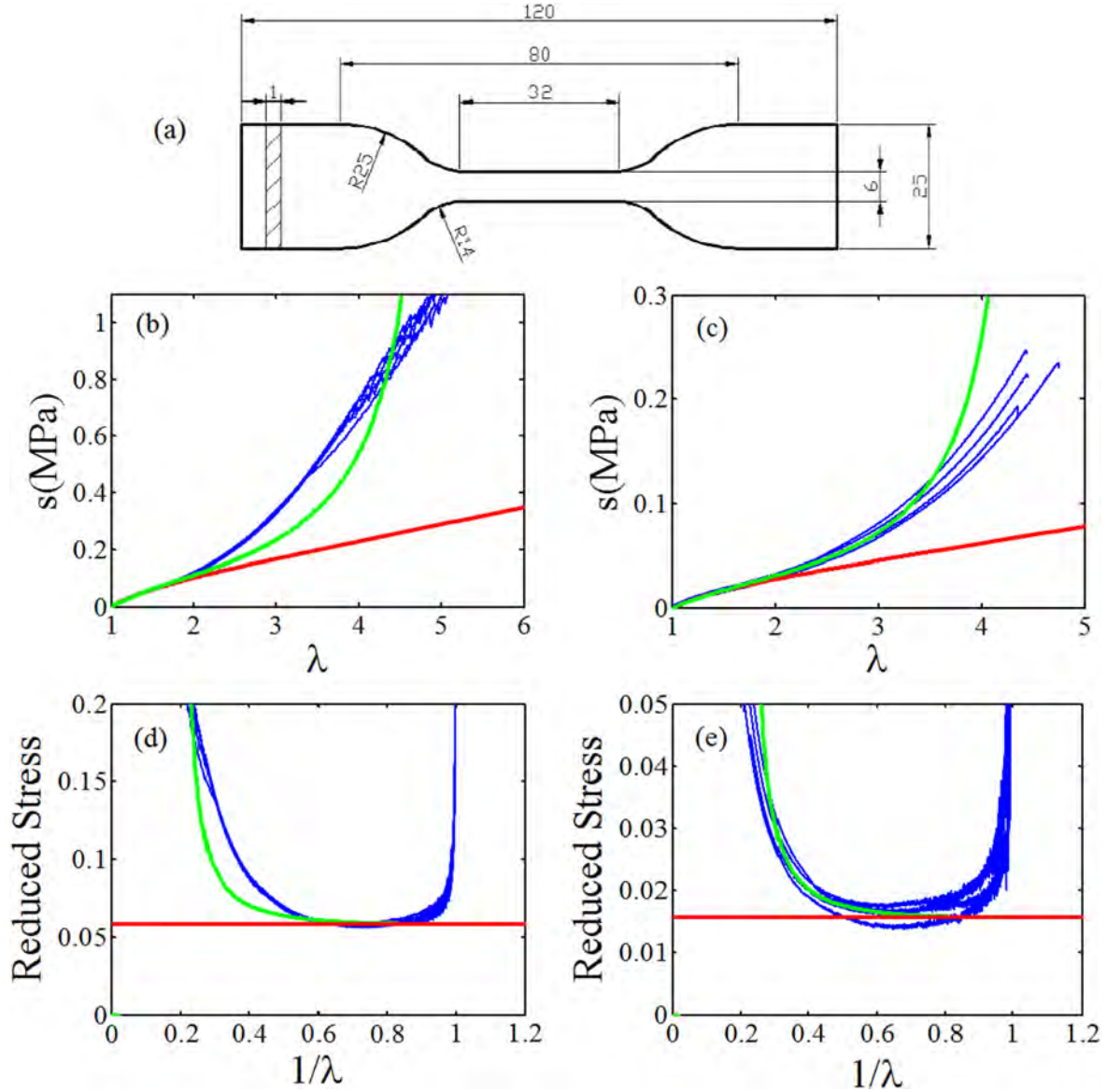


**Figure 4.** Specimen Size (a) Data Fitting Results of 20% Silicone Rubber (b) and 40% Silicone Rubber (c) Mooney plot of 20% Silicone Rubber (d) and 40% Silicone Rubber (e).

**Table 1.** Data Fitting Results.

	$\mu$ (kPa)	$\lambda_{lim}$	$J_{lim}$
20% Silicone Rubber	58.26	5.1	23.4
40% Silicone Rubber	15.63	4.5	17.69

$$\frac{\tilde{E}}{\sqrt{\mu/\varepsilon}} = \frac{\tilde{D}}{\sqrt{\mu\varepsilon}} \lambda^{-4} \quad (10)$$

deformation means more converted energy. Therefore, we choose Gent model here.

From the state equations of the ideal incompressible DE film undergoing equal-biaxial stretch

$$\frac{s}{\mu} = \frac{J_{lim}(\lambda - \lambda^{-5})}{J_{lim} - 2\lambda^2 - \lambda^{-4} + 3} - \frac{\tilde{D}^2}{\mu\varepsilon} \lambda^{-5} \quad (9)$$

The failure modes are seen as the normal working critical conditions [5, 21, 23], and in the following analysis, we make  $S = \frac{s}{\mu}$ ,  $U = \frac{\tilde{E}}{\sqrt{\mu/\varepsilon}}$  and  $Q = \frac{\tilde{D}}{\sqrt{\mu\varepsilon}}$ .

**(1) Loss of Charge (LC).** In this condition, the DE film is uncharged,  $\tilde{E} = 0$  and  $\tilde{D} = 0$ , equations (9) and (10) become

$$S = \frac{J_{lim}(\lambda - \lambda^{-5})}{J_{lim} - 2\lambda^2 - \lambda^{-4} + 3} \quad (11)$$

$$U = Q = 0 \quad (12)$$

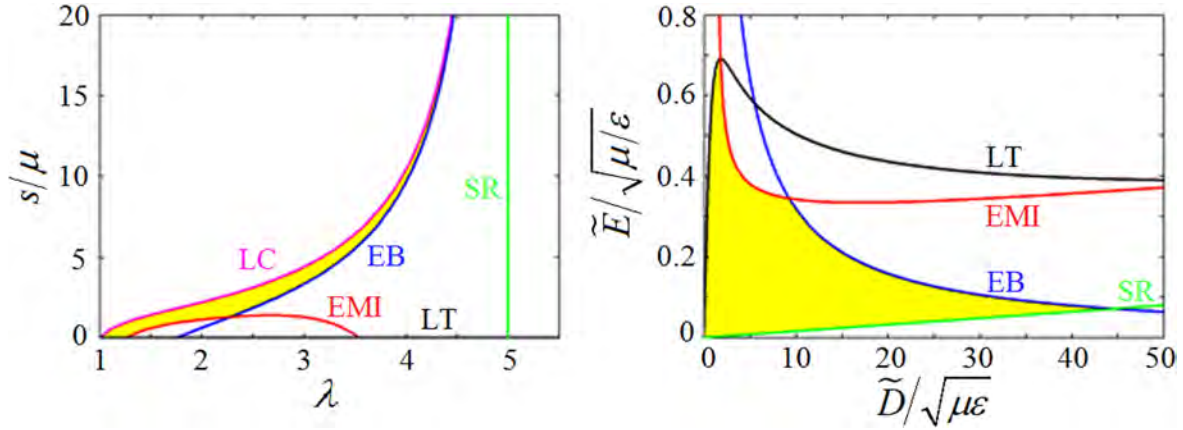


Figure 5. Allowable Areas in Work-Conjugate Coordinates.

In force-displacement plane, the LC curve is the upper boundary of allowable area; and in voltage-charge plane, it degenerates to the origin of coordinates.

(2) **Electrical Breakdown (EB)**. When the electric field overloads, the accumulation of enough quantity of charged particles will cause the DE material loss its insulativity, we call it electrical breakdown. Assuming the critical electric field is  $E_{EB}$ , and the nominal electric field is  $\tilde{E} = E_{EB}\lambda^{-2}$ , equations (9) and (10) can be

$$S = \frac{J_{lim}(\lambda - \lambda^{-5})}{J_{lim} - 2\lambda^2 - \lambda^{-4} + 3} - \frac{E_{EB}^2}{\mu/\epsilon}\lambda^{-1} \quad (13)$$

$$U = \left(\frac{E_{EB}^2}{\mu/\epsilon}\right)Q^{-1} \quad (14)$$

In force-displacement plane, allowable area is above the EB curve; and in voltage-charge plane, it is under the EB curve.

(3) **Electromechanical Instability (EMI)**. When the electric field is smaller than the electrical breakdown field, but reaches some critical value, a material instability may occur. The critical electric field leads to a thinner film and the thinner film simultaneously leads to a higher true electric field, this positive feedback will continuously increase the electric field until the electrical breakdown happens [11]. The boundary equations can be derived in the following method: utilize equation (10) to eliminate  $\tilde{D}$  in equation (9); express  $\tilde{E}$  as a function of  $\lambda$  and  $s$ ; then regard  $s$  as a constant; make the derivative of  $\tilde{E}(\lambda, s)$  be 0, and we can get

$$S = \left( J_{lim} \left[ 4\lambda^{-9} - (8J_{lim} + 24)\lambda^{-5} + 22\lambda^{-3} + (2J_{lim} + 6)\lambda - 8\lambda^3 \right] / \left( 3(J_{lim} - 2\lambda^2 - \lambda^{-4} + 3)^2 \right) \right) \quad (15)$$

The maximal electric field corresponds to the starting point of EMI. Combine equations (9), (10) and (15)

$$\begin{aligned} & 3Q^2 \left[ J_{lim} - 2\left(\frac{U}{Q}\right)^{-\frac{1}{2}} - \frac{U}{Q} + 3 \right]^2 \\ & = J_{lim} \left[ -\frac{U}{Q} + (5J_{lim} + 15) - 19\left(\frac{U}{Q}\right)^{-\frac{1}{2}} + (J_{lim} + 3)\left(\frac{U}{Q}\right)^{-\frac{3}{2}} + 2\left(\frac{U}{Q}\right)^{-2} \right] \end{aligned} \quad (16)$$

In force-displacement plane, the area above the EMI curve is allowable; and in voltage-charge plane, the lower area is allowable.

(4) **Loss of Tension(LT)**. In this condition, the DE film is under no load, equations (9) and (10) can be

$$S = 0 \quad (17)$$

$$\begin{aligned} & J_{lim} \left(\frac{U}{Q}\right)^{-\frac{3}{2}} + 2Q^2 \left(\frac{U}{Q}\right)^{-\frac{1}{2}} + Q^2 \left(\frac{U}{Q}\right) \\ & - (3Q^2 + J_{lim} + J_{lim}Q^2) = 0 \end{aligned} \quad (18)$$

The LT curve and x-coordinate overlap in force-displacement plane, the upper part of which is the allowable area; and in voltage-charge plane, the allowable area is under that curve.

(5) **Stretch Rupture(Sr)**. When the mechanical force overloads, the DE film will rupture. In Gent model, limiting stretch ( $\lambda_{lim}$ ) restricts the maximal deformation of dielectric elastomer. Therefore, equations (9) and (10) become

$$\lambda = \lambda_{lim} \quad (19)$$

$$U = \lambda_{lim}^{-4} Q \quad (20)$$

The Sr curve is vertical to the x-coordinate in force-displacement plane, the left part is the allowable area; and the allowable area is above the Sr curve in voltage-charge plane.

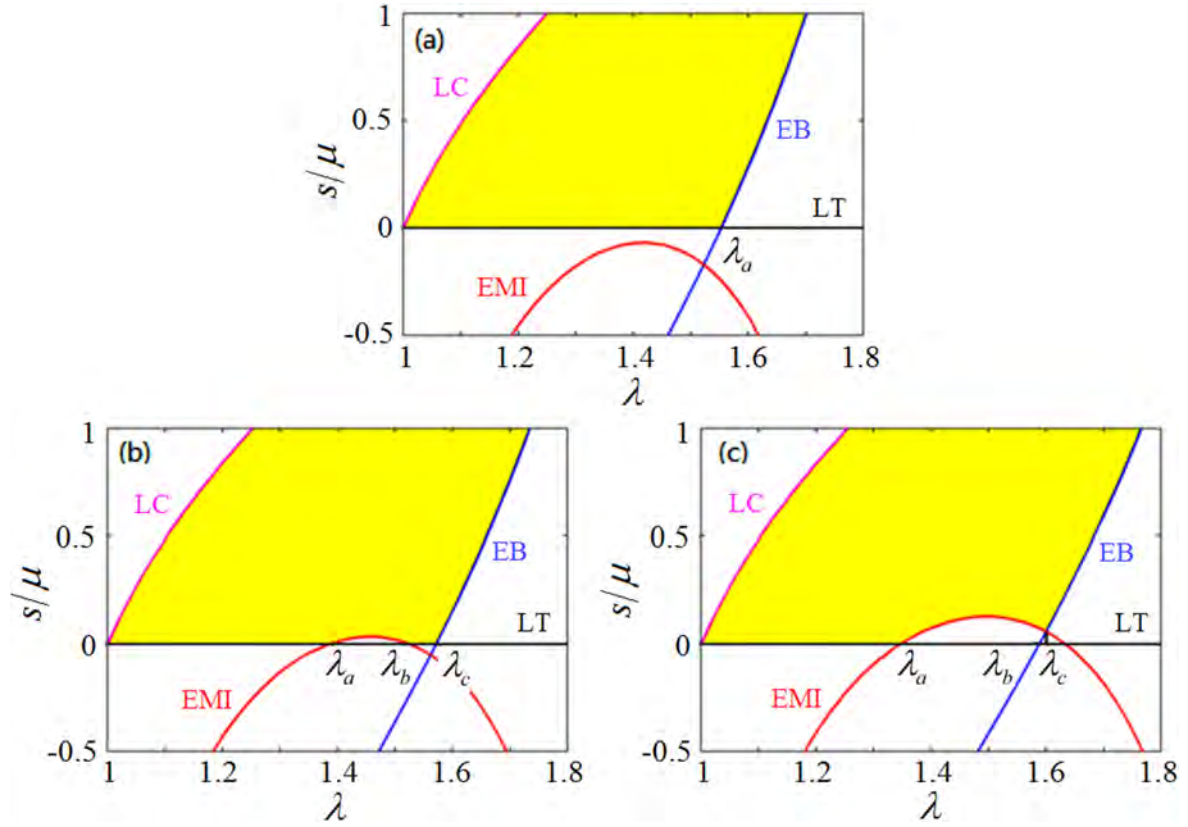


Figure 6. Position Relationships in Force-Displacement Plane.

According to equations (11) to (20), by choosing the typical parameters ( $\lambda_{lim} = 5$ ,  $\mu = 10^3$  kPa and  $\varepsilon = 3.54 \times 10^{-11}$  F m $^{-1}$  [21]), we can depict the allowable areas in planes of work-conjugate coordinates (figure 5). For a DE generator, the allowable areas represent the input mechanical energy and the output electrical energy in force-displacement plane and voltage-charge plane, respectively. Because of the equal-biaxial stretch, the allowable area in voltage-charge plane should be twice of that in force-displacement plane.

Energy density is the physical quantity that reflects the ability to convert energy of a certain material per unit mass. Under equal-biaxial stretch, the energy density can be expressed

$$Y = 2\mu A_{P-L}/\rho = \mu A_{U-Q}/\rho \quad (21)$$

Considering the simplicity of calculation, here we make  $\rho = 1000$  kg m $^{-3}$ .

Ideally, the input mechanical energy can be absolutely converted into the output electrical energy. So we can calculate the maximal converted energy from the both two planes. Here we commence it from the force-displacement plane.

The position relationship of these boundary curves changes along with  $\lambda_{lim}$ . When  $\lambda_{lim}$  is relatively small, the EMI curve has no intersection point with the allowable area,

as shown in figure 6(a). We can express the allowable area

$$\begin{aligned} A &= \int_1^{\lambda_{lim}} S_{LC}(\lambda) d\lambda - \int_{\lambda_a}^{\lambda_{lim}} S_{EB}(\lambda) d\lambda \\ &= -\frac{1}{4} J_{lim} \ln (J_{lim} - 2\lambda^2 - \lambda^{-4} + 3) \Big|_1^{\lambda_a} \\ &\quad + \frac{E_{EB}^2}{\mu/\varepsilon} \ln \lambda \Big|_{\lambda_a}^{\lambda_{lim}} \end{aligned} \quad (22)$$

With the increase of  $\lambda_{lim}$ , the EMI curve moves up, and it will intersect with the LT curve at first. The two intersection points are between the LC and EB curves, as shown in figure 6(b). The allowable area can be expressed

$$\begin{aligned} A &= \int_1^{\lambda_{lim}} S_{LC}(\lambda) d\lambda - \int_{\lambda_c}^{\lambda_{lim}} S_{EB}(\lambda) d\lambda - \int_{\lambda_a}^{\lambda_b} S_{EMI}(\lambda) d\lambda \\ &= \frac{1}{3} \left[ \frac{J_{lim}(\lambda^2 - \lambda^{-4})}{J_{lim} - 2\lambda^2 - \lambda^{-4} + 3} \right] \\ &\quad + J_{lim} \ln (J_{lim} - 2\lambda^2 - \lambda^{-4} + 3) \Big|_{\lambda_a}^{\lambda_b} + \frac{E_{EB}^2}{\mu/\varepsilon} \ln \lambda \Big|_{\lambda_c}^{\lambda_{lim}} \\ &\quad - \frac{1}{4} J_{lim} \ln (J_{lim} - 2\lambda^2 - \lambda^{-4} + 3) \Big|_1^{\lambda_c} \end{aligned} \quad (23)$$

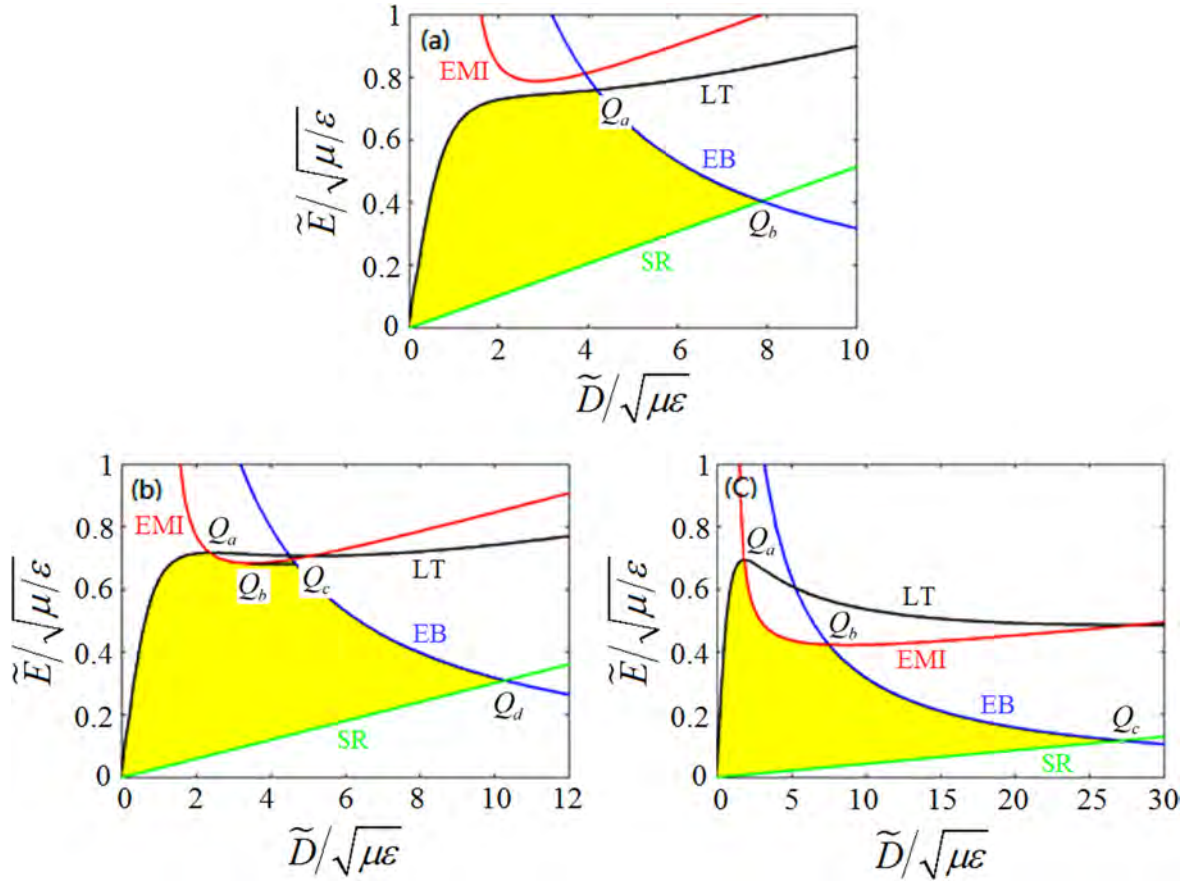


Figure 7. Position Relationships in Voltage-Charge Plane.

After that, the right intersection point will go across the EB curve as the EMI curve continues to move up (figure 6(c)). We have the allowable area

$$\begin{aligned}
 A &= \int_1^{\lambda_{\text{lim}}} S_{LC}(\lambda) d\lambda - \int_{\lambda_b}^{\lambda_{\text{lim}}} S_{EB}(\lambda) d\lambda \\
 &\quad - \left[ \int_{\lambda_a}^{\lambda_c} S_{EMI}(\lambda) d\lambda - \int_{\lambda_b}^{\lambda_c} S_{EB}(\lambda) d\lambda \right] \\
 &= \frac{1}{3} \left[ \frac{J_{\text{lim}}(\lambda^2 - \lambda^4)}{J_{\text{lim}} - 2\lambda^2 - \lambda^4 + 3} \right. \\
 &\quad \left. + J_{\text{lim}} \ln(J_{\text{lim}} - 2\lambda^2 - \lambda^4 + 3) \right] \Big|_{\lambda_a}^{\lambda_c} + \frac{E_{EB}^2}{\mu/\varepsilon} \ln \lambda \Big|_{\lambda_c}^{\lambda_{\text{lim}}} \\
 &\quad - \frac{1}{4} J_{\text{lim}} \ln(J_{\text{lim}} - 2\lambda^2 - \lambda^4 + 3) \Big|_1^{\lambda_c} \quad (24)
 \end{aligned}$$

To obtain the ideal maximal converted energy, we should precisely control the energy harvesting process to go along with the boundary curves. But in fact we cannot achieve the most optimal energy harvesting process. Therefore, we calculate the maximal converted energy of a rectangular cycle proposed by Koh *et al* [21]. According to the energy harvesting principle, the voltage and charge change are both caused by the capacitance change, and the charge change is

prior to the voltage change. Therefore, the voltage change range cannot exceed the charge change range. That is, in allowable area, the vertical side is smaller than the horizontal side. We can find such a rectangle to analyze the maximal converted energy.

Making the x-coordinate  $Q$  of the Sr curve as the reference point, we can express the rectangular area. When  $\lambda_{\text{lim}}$  is relatively small, the EB curve and LT curve intersect at  $Q_a$ , and the EB curve and Sr curve intersect at  $Q_b$ . Thus,  $Q$  must be between  $Q_a$  and  $Q_b$  (figure 7(a)).

$$A_R = [U_{EB}(Q) - U_{SR}(Q)][Q - Q_{LT}(U_{EB}(Q))] \quad (25)$$

As  $\lambda_{\text{lim}}$  increases, the EMI curve and LT curve intersect at  $Q_a$ , and the minimum point of the EMI curve is  $Q_b$ ; the point that has same y-coordinate with  $Q_b$  on the EB curve is  $Q_c$ , and the EB curve and Sr curve intersect at  $Q_d$ . Thus,  $Q$  must be between  $Q_a$  and  $Q_b$  or  $Q_c$  and  $Q_d$  (figure 7(b)).

when  $Q_a < Q < Q_b$

$$A_R = [U_{EMI}(Q) - U_{SR}(Q)][Q - Q_{LT}(U_{EMI}(Q))] \quad (26)$$

when  $Q_c < Q < Q_d$

$$A_R = [U_{EB}(Q) - U_{SR}(Q)][Q - Q_{LT}(U_{EB}(Q))] \quad (27)$$

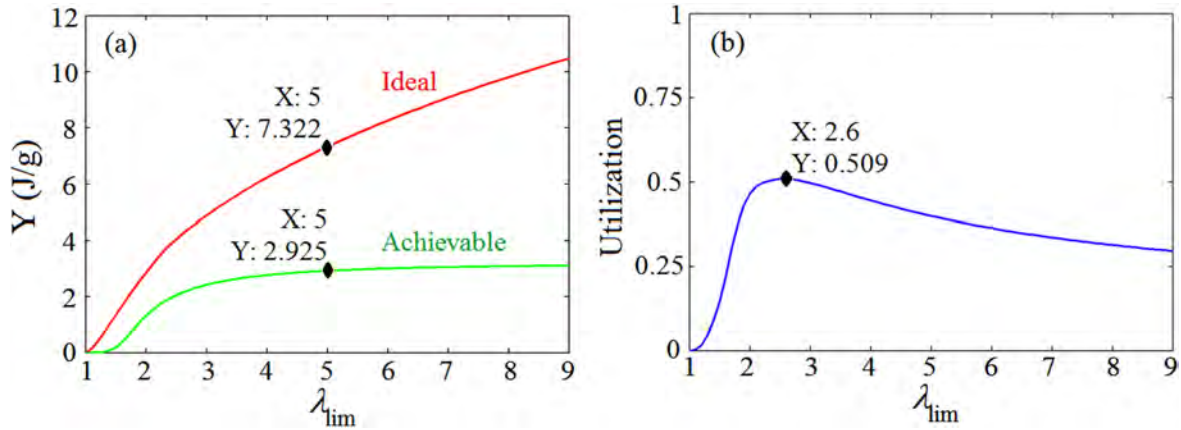


Figure 8. Energy Density-Limiting Stretch Curves (a) and Utilization-Limiting Stretch Curve (b).

After that, the EMI curve and LT curve intersect at  $Q_a$ , and the EMI curve and EB curve intersect at  $Q_b$ ; and the minimum point of the EMI curve is on the right side of the EB curve, and the EB curve and Sr curve intersect at  $Q_c$ . Thus,  $Q$  must be between  $Q_a$  and  $Q_c$  (figure 7(c)).

when  $Q_a < Q < Q_b$

$$A_R = [U_{EMI}(Q) - U_{SR}(Q)][Q - Q_{LT}(U_{EMI}(Q))] \quad (28)$$

when  $Q_b < Q < Q_c$

$$A_R = [U_{EB}(Q) - U_{SR}(Q)][Q - Q_{LT}(U_{EB}(Q))] \quad (29)$$

The symbols  $S_{(LC,EB,EMI)}(\lambda)$ ,  $U_{(Sr,EB,EMI)}(Q)$  and  $Q_{LT}(U)$  in equations (22) to (29) represent the boundary curves of each failure mode. They are the function of  $\lambda$ ,  $Q$  and  $U$ .

Equations (22) to (24) give the calculation formulas of the whole allowable area with different  $\lambda_{lim}$ . Combine with equation (21), the ideal maximal energy density versus limiting stretch curve can be obtained. Equations (25) to (29) give the calculation formulas of the rectangular area with different  $\lambda_{lim}$ . The boundary curve equations in these formulas have been given (equations (14), (16), (18) and (20)), so the corresponding rectangular areas are available after substituting them into these formulas. The area contains an unknown quantity  $Q$ , so different values will be obtained, and among them, a maximal  $S$  must exist. Combine with equation (21), the rectangular maximal energy density versus limiting stretch curve can be obtained.

Finally, we can get the maximal energy density in figure 8(a). The slope of both curves decreases as limiting stretch increases. This means when the limiting stretch increases, the increment of energy decreases; but when it increases to some degree, this energy density will almost remain at a constant level. When  $\lambda_{lim} = 5$ , the ideal maximal energy density is  $7.322 \text{ J g}^{-1}$  and the rectangular maximal energy density is  $2.925 \text{ J g}^{-1}$ . The result of Gent model is a little bigger than that of neo-Hookean model. This is caused by the differences between the two material models. In force-displacement plane, Gent model extends to the upper right region in the form of limit and infinitely tends to the limiting stretch; while neo-Hookean model is cut off by the limiting

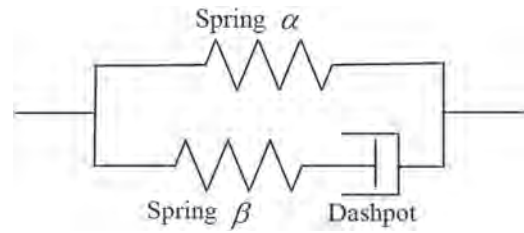


Figure 9. Viscoelastic Model.

stretch with a finite length. For the ideal case, the material performance is fully utilized. While for the rectangular energy harvesting cycle, figure 8(b) shows the utilization of material performance. When  $\lambda_{lim} = 2.6$ , the utilization is the highest, reaching 50.9%. However, when  $\lambda_{lim} = 5$ , the utilization is only 39.95%.

#### 4. Viscoelastic dissipation

The mechanical model of spring and dashpot (figure 9) is used to describe the viscoelastic behavior of dielectric elastomer here [24–27]. Make the stretch of spring  $\alpha$  and dashpot be  $\lambda$  and  $\xi$ , respectively. By geometry,  $\lambda$  is the stretch of DE film and  $\lambda\xi^{-1}$  is the stretch of spring  $\beta$ . Regarding  $\xi$  as the internal variable, the free energy density of the system consists of the elastic strain energy of the two springs and the static electrical energy. For simplicity, neo-Hookean model is used.

$$\begin{aligned} W(\lambda_1, \lambda_2, \tilde{D}, \xi_1, \xi_2) &= \frac{\mu_\alpha}{2} (\lambda_1^2 + \lambda_2^2 + \lambda_1^{-2}\lambda_2^{-2} - 3) \\ &+ \frac{\mu_\beta}{2} (\lambda_1^2\xi_1^{-2} + \lambda_2^2\xi_2^{-2} + \lambda_1^{-2}\xi_1^2\lambda_2^{-2}\xi_2^2 - 3) \\ &+ \frac{\tilde{D}^2}{2\varepsilon} \lambda_1^{-2}\lambda_2^{-2} \end{aligned} \quad (30)$$

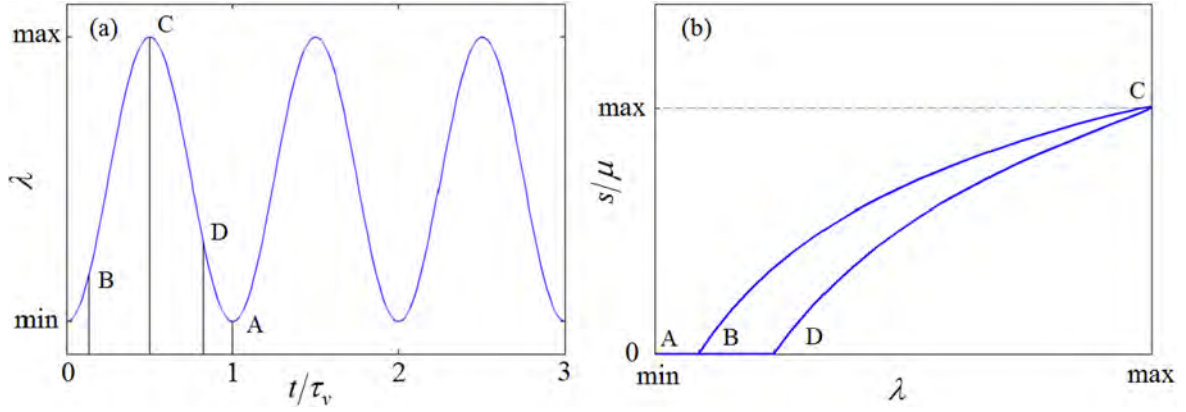


Figure 10. Sine Deformation (a) and Cycle in force—displacement Plane (b).

The state equation under equal-biaxial stretch is

$$s = \mu_\alpha(\lambda - \lambda^{-5}) + \mu_\beta(\lambda\xi^{-2} - \lambda^{-5}\xi^4) - \frac{\tilde{D}^2}{\varepsilon}\lambda^{-5} \quad (31)$$

Due to the dashpot and spring  $\beta$  are in series, the true stress of them is same. The true stress in spring  $\beta$  is

$$\sigma_\beta = \lambda s_\beta = \mu_\beta(\lambda^2\xi^{-2} - \lambda^{-4}\xi^4) \quad (32)$$

The deformation rate of dashpot is

$$\xi^{-1}d\xi/dt \quad (33)$$

So

$$\frac{d\xi}{dt} = \frac{\mu_\beta}{\eta}(\lambda^2\xi^{-1} - \lambda^{-4}\xi^5) \quad (34)$$

Define  $\tau_v = \eta/\mu_\beta$  to be the relaxation time, then  $T = t/\tau_v$  is the dimensionless time, and make  $\mu_\alpha = \mu_\beta = \mu$ , equations (31) and (34) become

$$\lambda - \lambda^{-5} + \lambda\xi^{-2} - \lambda^{-5}\xi^4 - \frac{\tilde{E}^2}{\mu/\varepsilon}\lambda^3 - \frac{s}{\mu} = 0 \quad (35)$$

$$\dot{\xi} = \lambda^2\xi^{-1} - \lambda^{-4}\xi^5 \quad (36)$$

$\lambda$ ,  $\xi$ ,  $\tilde{E}$  and  $s$  are the functions of  $T$ , and then we can have

$$\begin{aligned} & \dot{\lambda} + 5\lambda^{-6}\dot{\lambda} + \xi^{-2}\dot{\lambda} - 2\lambda\xi^{-3}\dot{\xi} + 5\lambda^{-6}\xi^4\dot{\lambda} \\ & - 4\lambda^{-5}\xi^3\dot{\xi} - \frac{3\tilde{E}^2}{\mu/\varepsilon}\lambda^2\dot{\lambda} - \frac{2\tilde{E}\dot{\tilde{E}}}{\mu/\varepsilon}\lambda^3 - \frac{\dot{s}}{\mu} = 0 \end{aligned} \quad (37)$$

Equations (36) and (37) are two differential equations which contain four unknown functions. If we know two of the four, we can get the other two.

In the energy harvesting process, the deformation of DE film can be simplified to a sine form (figure 10(a)).

$$\lambda(t) = \left( \frac{\lambda_{\max} - \lambda_{\min}}{2} \right) \sin\left( \frac{2\pi}{t_{\text{cycle}}}t - \frac{\pi}{2} \right) + \frac{\lambda_{\max} + \lambda_{\min}}{2} \quad (38)$$

So the problem is to solve the viscoelastic response under the given sine deformation. Due to the neo-Hookean model being only suitable for small stretch, here we choose  $\lambda_{\min} = 1$  and  $\lambda_{\max} = 2$ . In addition, to reflect the time dependence of viscoelastic effect, we choose different  $t_{\text{cycle}}$  ( $0.01\tau_v$ ,  $0.1\tau_v$ ,  $\tau_v$  and  $10\tau_v$ ).

The viscoelastic effect exists all the time. So, the initial condition

$$\xi(0) = 1 \quad (39)$$

This process is divided into four stages (figure 10). In stage A-B ( $t_0 < t < t_1$ ), the DE film is charged by an external power  $U$ , so it has an initial stretch

$$s = 0 \quad (40)$$

$$\frac{\varepsilon U_{DE}^2}{\mu H^2} = \lambda(t)^{-2} - \lambda(t)^{-8} + \lambda(t)^{-2}\xi(t)^{-2} - \lambda(t)^{-8}\xi(t)^4 \quad (41)$$

where  $U_{DE}$  is the voltage across the DE film. When  $U_{DE} = U$  ( $t = t_1$ ), the charging process completes.

In stage B-C ( $t_1 < t < t_2$ ), keep the voltage  $U_{DE} = U$  constant, the DE film is loaded to a maximal stretch  $\lambda_{\max}$

$$\frac{s}{\mu} = \lambda - \lambda^{-5} + \lambda\xi^{-2} - \lambda^{-5}\xi^4 - \frac{\varepsilon U^2}{\mu H^2}\lambda^3 \quad (42)$$

where

$$\frac{\varepsilon U^2}{\mu H^2} = \lambda(t_1)^{-2} - \lambda(t_1)^{-8} + \lambda(t_1)^{-2}\xi(t_1)^{-2} - \lambda(t_1)^{-8}\xi(t_1)^4 \quad (43)$$

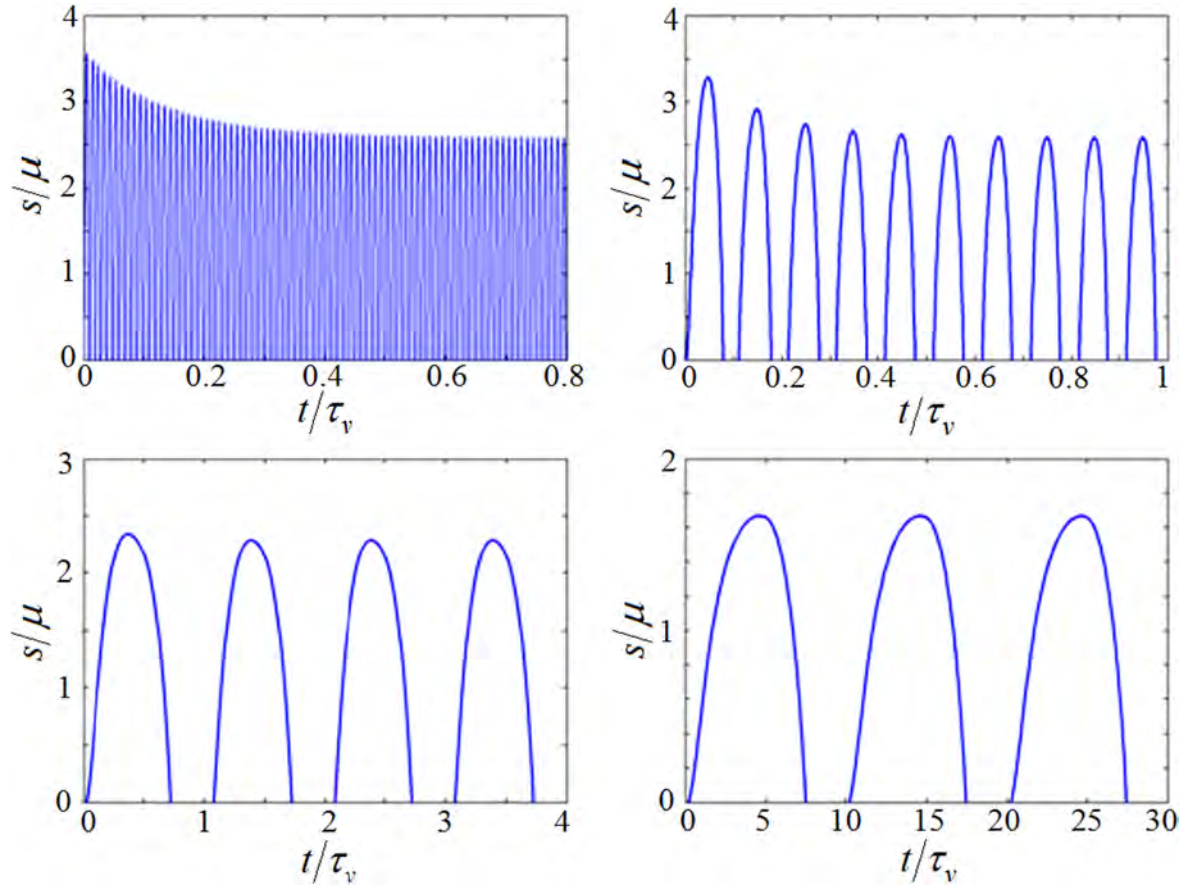


Figure 11. Load-Time Curves of DE Film.

In stage C-D ( $t_2 < t < t_3$ ), the external power is disconnected. Keep the total charge  $Q$  constant, the DE film is completely unloaded to a residual stretch

$$\frac{s}{\mu} = \lambda - \lambda^{-5} + \lambda \xi^{-2} - \lambda^{-5} \xi^4 - \frac{Q^2}{\mu \varepsilon L^4} \lambda^{-5} \quad (44)$$

where

$$\frac{Q^2}{\mu \varepsilon L^4} = \lambda_{\max}^6 - 1 + \lambda_{\max}^6 \xi(t_2)^{-2} - \xi^4 - \frac{s(t_2)}{\mu} \lambda_{\max}^5 \quad (45)$$

In stage D-A ( $t_3 < t < t_4$ ), the external circuit is connected, the total charge  $Q$  and voltage  $U_{DE}$  reduce to 0, and the stretch reduces to  $\lambda_{\min}$

$$s = 0 \quad (46)$$

$$\frac{\varepsilon U_{DE}^2}{\mu H^2} = \lambda(t)^{-2} - \lambda(t)^{-8} + \lambda(t)^{-2} \xi(t)^{-2} - \lambda(t)^{-8} \xi(t)^4 \quad (47)$$

where  $U_{DE}$  is the voltage across the DE film. When  $U_{DE} = 0$  ( $t = t_4$ ), the discharging process completes.

In the state equations, we make  $\varepsilon U^2 / \mu H^2 = 0.04$ ,  $\lambda_{\min}$ ,  $\lambda_{\max}$  and  $t_{\text{cycle}}$  are all similar to the above analysis. Figures 11

to 14 give the load-time curves and load-stretch curves of DE film and dashpot, respectively.

From figures 11 and 12, due to the viscoelasticity, the energy harvesting cycle needs several periods to get stable. After stability, the load-stretch curves in every period will coincide, and the closed area represents the input mechanical energy in every period. We also give the limiting curves in figure 12, it shows that the energy harvesting cycle exceeds the allowable area when cycle time is long. It means that faster cycle time may avoid EMI.

From figures 13 and 14, after stability, the load-stretch curves will encircle an area which represents the dissipative mechanical energy in every period. The shorter the period, the greater the cycle times to achieve stability. But the dissipative mechanical energy in each period is less.

## 5. Wave power generator

Figure 15 is the schematic diagram of the wave power generator. The round stacked DE transducers are made of silicone rubber with C fraction of 40%,  $\varepsilon = 2.74 \times 10^4 \text{ F m}^{-1}$ ,  $\rho = 1.05 \times 10^6 \text{ g m}^{-3}$ . The height of each transducer is about 35 mm with 30 layers. The transducer diameter is 60 mm, while the electrode diameter is 40 mm. The transducers are placed in three symmetric sleeves and connected in parallel. The sleeves together with an upper board, a lower

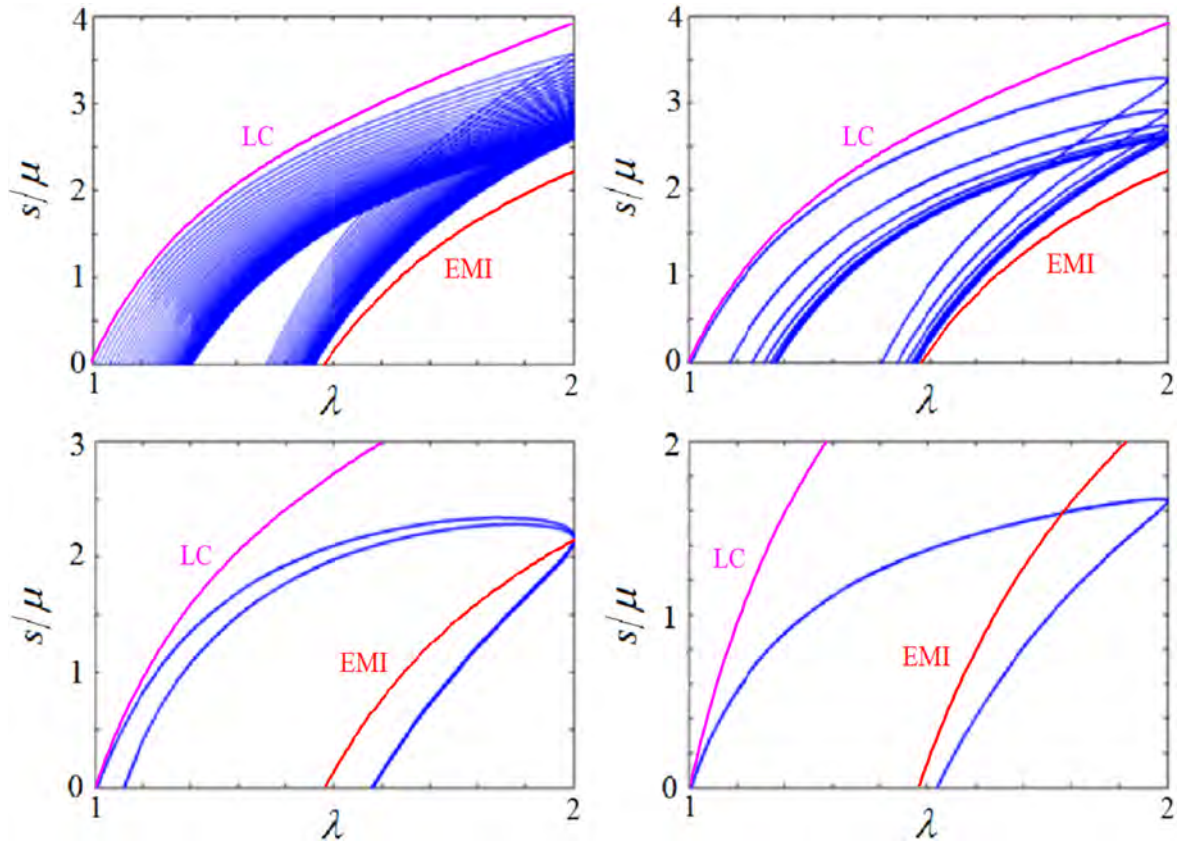


Figure 12. Load- Stretch Curves of DE Film.

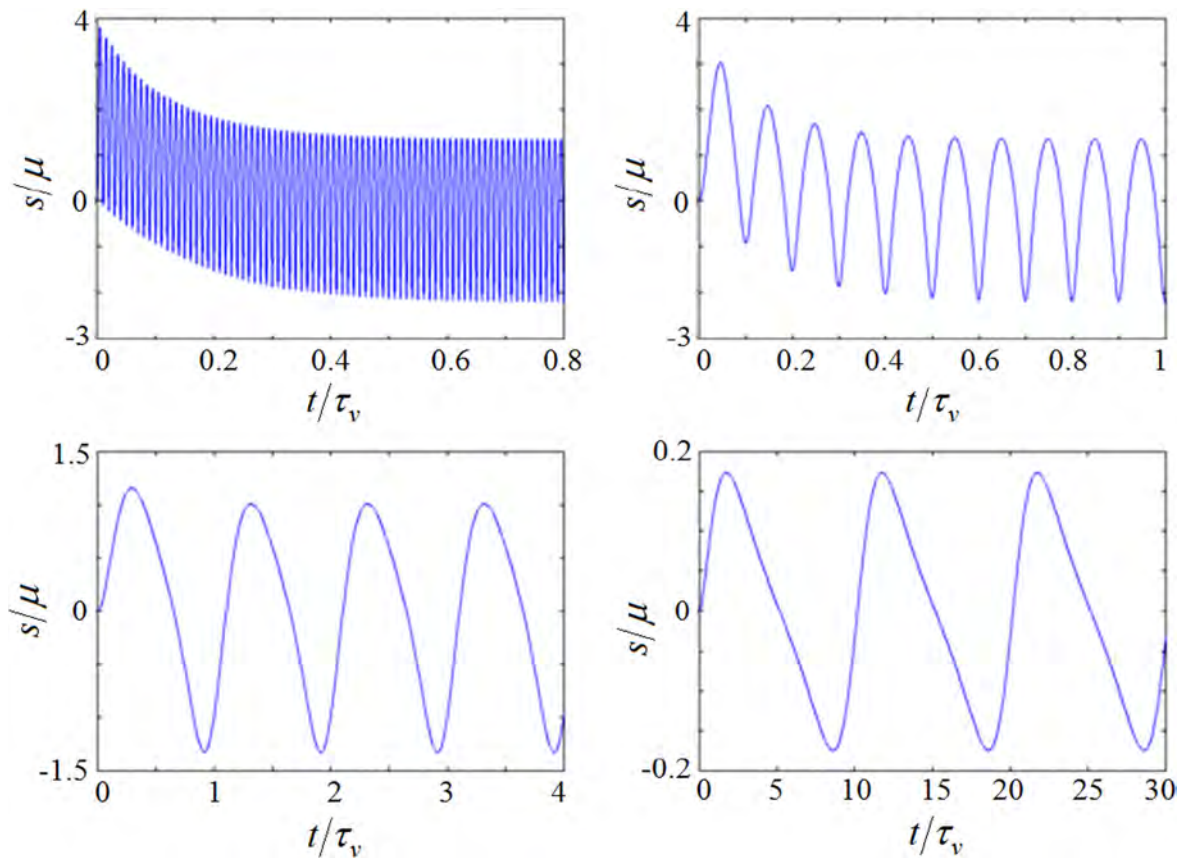


Figure 13. Load-Time Curves of Dashpot.

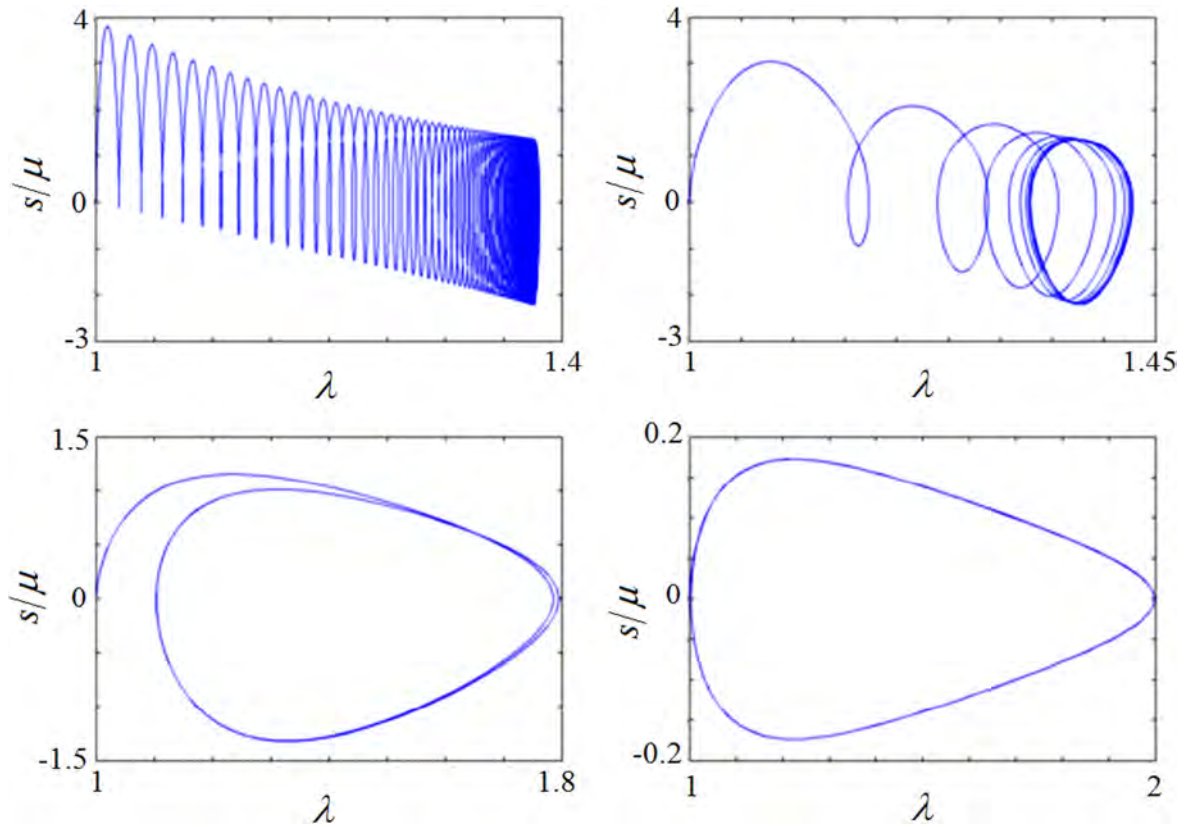


Figure 14. Load- Stretch Curves of Dashpot.

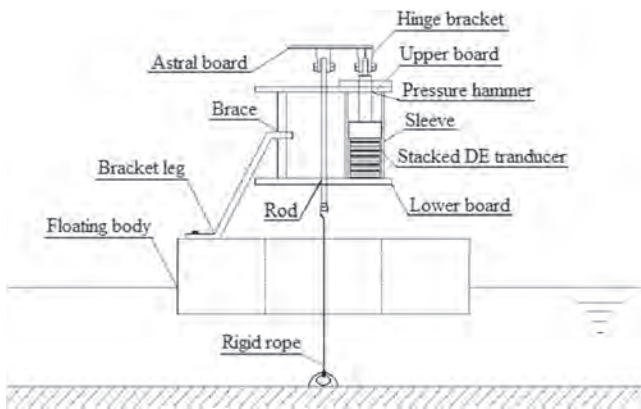


Figure 15. Schematic Diagram of Wave Power Generator.

board and three braces are connected to a floating body through three bracket legs. In each sleeve, there is a pressure hammer which is hinged on the corner of an astral board. The astral board is hinged with a rod which is connected to a rigid rope through the center hole of the upper and lower board; the other end of the rope is firmly tied to the bottom.

When there are waves, the floating body will drive the sleeves up and down. However, the pressure hammer is connected to the bottom; it cannot move sharply. Consequently, the stacked DE transducers will be compressed repeatedly and mechanical energy will input over and over again. After the conversion, the output energy is consumed



Figure 16. Operating Platform.

through a pair of resistances with the capacity of 100 K and 200 M in series.

Next, we establish an operating platform (figure 16). A small motor is solidly fixed to drive a foam board up and down through the mechanism of disc and rod. A high-voltage amplifier is used to supply high voltage to the generator. The output voltage is monitored by an oscilloscope paralleled to the smaller resistance. Figure 17 gives the output voltage

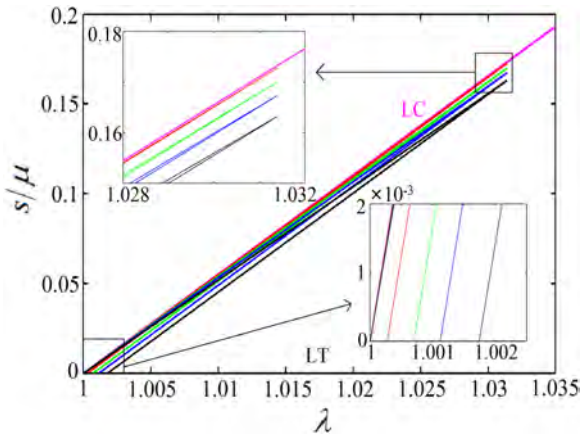


Figure 17. Energy Harvesting Cycle in Force-Displacement Plane.

change corresponds to different input voltages, the converted energy can be determined by

$$E = \int_0^T \frac{U_{Output}(t)^2}{R} dt - \frac{1}{2} C_1 U^2 \quad (48)$$

Where  $C_2$  and  $C_1$  are the capacitances before and after deformation,  $U$  is the input voltage and  $t$  is the output time. The measured initial capacitance is about 3.3 nF, and the approximate discharge time is 2 s.

For compression of the stacked transducers,  $\lambda = \lambda_1 = \lambda_2 = \lambda_3^{-0.5}$  and  $s = s_1 = s_2 = \lambda^{-3} s_3$ , so we can

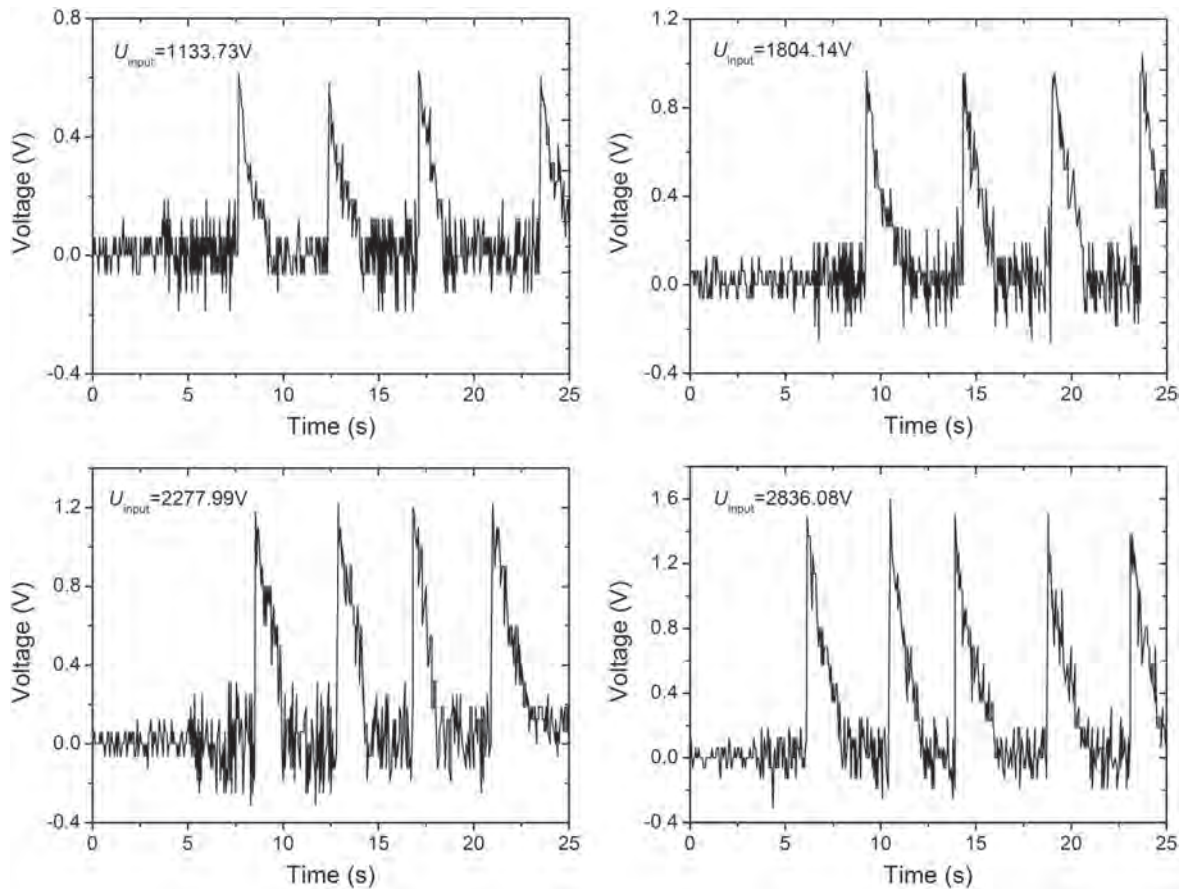


Figure 18. Output Voltage across the 100 K Capacitance.

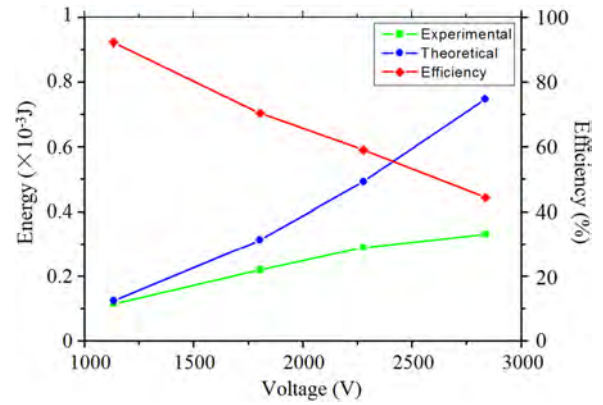


Figure 19. Converted Energy and Efficiency.

change it to equal-biaxial stretch. The compression of the transducer is 2 mm, so  $\lambda = 1.0314$ . The loading and unloading path can be drawn in force-displacement plane (figure 18). We can get the energy density under different input voltages. Because of small deformation and long relaxation time of our material, the calculated viscoelastic energy dissipation is several orders of magnitude smaller than energy density, so it is neglected here.

After calculation, results are shown in figure 19. The theoretical and experimental values increase along with the input energy. But the slope of the theoretical curve increases, while that of the experimental curve decreases, leading to the

conversion efficiency decreasing. The low converted energy is determined by the low capacitance and deformation of our transducers, the former is caused by the material property, while the latter is caused by the structure design. The gap between theoretical and experimental curves may be due to the large internal resistance and short discharge time, which lead to incomplete energy output, and the large energy dissipation caused by current leakage which is not studied in the paper. The decreasing efficiency may be mainly caused by the nonlinear current leakage increase when under higher voltage. It means that the dielectric property of the material also affects the performance of the DE generator.

## 6. Conclusion

The influence of Gent model and neo-Hookean model to the constitutive relation of DE materials was compared. As a result, they are almost identical under small stretch; and both are not exactly accurate under large stretch, but the trend of Gent model approaches the real situation.

Choosing Gent model, the ideal maximal energy density and rectangular maximal energy density were calculated, which are  $7.322 \text{ J g}^{-1}$  and  $2.925 \text{ J g}^{-1}$  at  $\lambda_{\text{lim}} = 5$ , respectively. The material utilization rate of the rectangle cycle does not increase as limiting stretch increases, reaching its maximal value about 50.9% at  $\lambda_{\text{lim}} = 2.6$ .

Choosing neo-Hookean model, the viscoelastic dissipation during fundamental energy harvesting process was analyzed. Results show that energy harvesting cycle needs several periods to achieve stability, and the times and dissipative energy is associated with the period.

A small wave power generator was designed and fabricated to achieve the energy conversion; and its performance was tested. The energy conversion efficiency of this generator decreases with the increasing input voltage. It may be mainly caused by the large current leakage under high voltage.

## Acknowledgments

This work is supported by the National Natural Science Foundation of China (Grant No.11225211, No.11272106, No.11102052).

## References

- [1] Krakovsky I, Romijn T and de Boer A P 1999 A few remarks on the electrostriction of elastomers *J. Appl. Phys.* **85** 628–9
- [2] Chu B J et al 2006 A dielectric polymer with high electric energy density and fast discharge speed *Science* **313** 334–6
- [3] Zhang Q M, Bharti V and Zhao X 1998 Giant electrostriction and relaxor ferroelectric behavior in electron-irradiated poly(vinylidene fluoride-trifluoroethylene) copolymer *Science* **280** 2101–4
- [4] Chiba S et al 2007 Extending applications of dielectric elastomer artificial muscle *Proceedings of SPIE*. **6524** 652424
- [5] Suo Z G 2010 Theory of dielectric elastomers *Acta Mech. Solida Sin.* **23** 549–78
- [6] Kornbluh R et al 2012 Dielectric elastomers: Stretching the capabilities of energy harvesting *MRS Bull.* **37** 246–53
- [7] Pelrine R et al 2001 Dielectric elastomers: generator mode fundamentals and applications *Proc. of SPIE*. **4329** 148–56
- [8] Suo Z G, Zhao X H and Greene W 2008 A nonlinear field theory of deformable dielectrics *J. Mech. Phys. Solids* **56** 467–86
- [9] Zhao X H, Hong W and Suo Z G 2007 Electromechanical hysteresis and coexistent states in dielectric elastomers *Phys. Rev. B* **76** 134113
- [10] Huang R and Suo Z G 2012 Electromechanical phase transition in dielectric elastomers *Proc. of the Royal Society A-Mathematical Physical and Engineering Sciences*. **468** 1014–40
- [11] Zhou J X et al 2008 Propagation of instability in dielectric elastomers *Int. J. of Solids and Structures*. **45** 3739–50
- [12] Zhao X H and Suo Z G 2007 Method to analyze electromechanical stability of dielectric elastomers *Appl. Phys. Lett.* **91** 061921
- [13] Liu Y J, Liu L W, Leng J S, Yu K and Sun S H 2009 Electromechanical stability of dielectric elastomer *Appl. Phys. Lett.* **95** 211901
- [14] Zhao X H and Suo Z G 2008 Electrostriction in elastic dielectrics undergoing large deformation *J. Appl. Phys.* **104** 123530
- [15] Li T F et al 2013 Giant voltage-induced deformation in dielectric elastomers near the verge of snap-through instability *J. Mech. Phys. Solids* **61** 611–28
- [16] Moscardo M, Zhao X H and Suo Z G 2008 On designing dielectric elastomer actuators *J. Appl. Phys.* **104** 093503
- [17] Zhu J, Cai S Q and Suo Z G 2010 Resonant behavior of a membrane of a dielectric elastomer *Int. J. of Solids and Structures*. **47** 3254–62
- [18] Zhao X H and Suo Z G 2008 Method to analyze programmable deformation of dielectric *Appl. Phys. Lett.* **93** 251902
- [19] Park H et al 2012 A dynamic finite element method for inhomogeneous deformation and electromechanical instability of dielectric elastomer transducers *Int. J. of Solids and Structures*. **49** 2187–94
- [20] Zhao X H, Koh S J A and Suo Z G 2011 Nonequilibrium thermodynamics of dielectric elastomers *Int. J. of Applied Mechanics* **3** 203–17
- [21] Koh S J A, Zhao X H and Suo Z G 2009 Maximal energy that can be converted by a dielectric elastomer generator *Appl. Phys. Lett.* **94** 262902
- [22] Kaltseis R et al 2011 Method for measuring energy generation and efficiency of dielectric elastomer generators *Appl. Phys. Lett.* **99** 162904
- [23] Liu Y J et al 2010 Analysis and manufacture of an energy harvester based on a mooney-Rivlin-type dielectric elastomer *Europhys. Lett.* **90** 36004
- [24] Hong W 2011 Modeling viscoelastic dielectrics *J. Mech. Phys. Solids* **59** 637–50
- [25] Foo C C et al 2012 Model of dissipative dielectric elastomers *J. Appl. Phys.* **111** 034102
- [26] Foo C C et al 2012 Performance of dissipative dielectric elastomer generators *J. Appl. Phys.* **111** 094107
- [27] Li T F, Qu S X and Yang W 2012 Energy harvesting of dielectric elastomer generators concerning inhomogeneous fields and viscoelastic deformation *J. Appl. Phys.* **112** 034119
- [28] Chiba S et al 2011 Current status and future prospects of power generators using dielectric elastomers *Smart Material and Structures* **20** 124006
- [29] Kornbluh R et al 2011 From boots to buoys: promises and challenges of dielectric elastomer energy harvesting *Proc. of SPIE*. **7976** 797605

- [30] Chiba S *et al* 2008 Innovative power generators for energy harvesting using electroactive polymer artificial muscles *Proc. of SPIE. San Diego: SPIE* **6927** 692715
- [31] Maas J and Graf C 2012 Dielectric elastomers for hydro power harvesting *Smart Mater. Struct.* **21** 064006
- [32] Gent N 1996 A new constitutive relation for rubber *Rubber Chemistry and Technology* **69** 59–61

# QUERY FORM

JOURNAL: Smart Materials and Structures

AUTHOR: X Lv *et al*

TITLE: Dielectric elastomer energy harvesting: maximal converted energy, viscoelastic dissipation and a wave power generator

ARTICLE ID: sms519958

---

---

The layout of this article has not yet been finalized. Therefore this proof may contain columns that are not fully balanced/matched or overlapping text in inline equations; these issues will be resolved once the final corrections have been incorporated.

---

SQ1

Please be aware that the colour figures in this article will only appear in colour in the online version. If you require colour in the printed journal and have not previously arranged it, please contact the Production Editor now.

---

We have been provided funding information for this article as below. Please confirm whether this information is correct. National Natural Science Foundation of China: Grant No.11225211, No.11272106, No.11102052.

**Page 1**

---

Q1

We have made a change to this sentence ‘...inspiration from bionics...’. Please review our edit.

**Page 14**

---

Q2

Please check the details for any journal references that do not have a link as they may contain some incorrect information.

---